strong constraints on different mixing processes (such as gravitational settling or meridional circulation).

Cosmic-ray nucleosynthesis models[24] and observations of interstellar clouds[25] indicate that the primordial ratio, $f(^6\mathrm{Li})$, in the protoplanetary matter could have been as high as 0.3–0.5, which in turn would allow either the possibility of some ^{6}Li depletion in the star or the ingestion of planets with even smaller mass. In this scenario we have assumed that the planet(s) was (were) ingested after the stellar convective envelope had shrunk, 10–30 Myr after stellar birth[19,5], and had reached its current mass and depth. The timescale is comparable to the lifetime of protoplanetary disks[26] (10–20 Myr) and planetary migration. Our results favour a scenario in which a planet was engulfed owing to the multi-body interactions in the system that can take place over a timescale of 100 Myr[27]. This is strongly supported by the highly eccentric orbit of the planetary companion of HD82943 (about 0.6). However, we hesitate to generalize it to explain the metal-rich nature[28,7] of other stars hosting planets. Further Li isotopic ratio studies of a large sample of planet-bearing stars can help to put additional constraints on this scenario.

Note added in proof: A second planet with a minimum mass of $0.88M_J$ has been discovered orbiting HD82943, with a period of 220 days (M. Mayor, personal communication). This detection has been done with the CORALIE spectrograph at the ESO La Silla Observatory. □

Received 3 November 2000; accepted 21 March 2001.

1. Weidenschilling, S. J. & Marzari, F. Gravitational scattering as a possible origin for giant planets at small distances. *Nature* **384,** 619–621 (1996).
2. Lin, D. N., Bodenheimer, P. & Richardson, D. C. Orbital migration of the planetary companion of 51 Pegasi to its present location. *Nature* **380,** 606–607 (1996).
3. Forestini, M. Low mass stars: Pre-main sequence evolution and nucleosynthesis. *Astron. Astrophys.* **285,** 473–488 (1994).
4. Andersen, J., Gustafsson, B. & Lambert, D. L. The lithium isotope ratio in F and G stars. *Astron. Astrophys.* **136,** 65–73 (1984).
5. Rebolo, R., Crivellari, L., Castelli, F., Foing, B. & Beckman, J. E. Lithium abundances and ^{7}Li/^{6}Li ratios in late-type population I field dwarfs. *Astron. Astrophys.* **166,** 195–203 (1986).
6. Naef, D. *et al.* The CORALIE survey for southern extrasolar planets V. 4 new extrasolar planets. *Astron. Astrophys.* (in the press).
7. Santos, N. C., Israelian, G. & Mayor, M. Chemical analysis of 8 recently discovered extra-solar planet host stars. *Astron. Astrophys.* **363,** 228–238 (2000).
8. Smith, V. V., Lambert, D. & Nissen, P. E. Isotopic lithium abundances in nine halo stars. *Astrophys. J.* **506,** 405–423 (1998).
9. Hobbs, L. M., Thorburn, J. A. & Rebull, L. M. Lithium isotope ratios in halo stars. III. *Astrophys. J.* **523,** 797–804 (1999).
10. Nissen, P. E., Lambert, D., Primas, F. & Smith, V. V. Isotopic lithium abundances in five metal-poor disk stars. *Astron. Astrophys.* **348,** 211–221 (1999).
11. Kurucz, R. L., Furenlid, I., Brault, J. & Testerman, L. Solar flux atlas from 296 to 1300 nm. *NOAO Atlas 1* (Harvard Univ. Press, Cambridge, Massachusetts, 1984).
12. Anders, E. & Grevesse, N. Abundances of the elements–meteoritic and solar. *Geochim. Cosmochim. Acta* **53,** 197–214 (1989).
13. Lambert, D., Smith, V. V. & Heath, J. Lithium in the barium stars. *Publ. Astron. Soc. Pacif.* **105,** 568–573 (1989).
14. Perryman, M. A. C. *et al.* The Hipparcos catalogue. *Astron. Astrophys. Lett.* **323,** 49–52 (1997).
15. Ramaty, R., Tatischeff, V., Thibaud, J. P., Kozlovsky, B. & Mandzhavidize, N. ^{6}Li from solar flares. *Astrophys. J. Lett.* **534,** 207–210 (2000).
16. Chaussidon, M. & Robert, F. Lithium nucleosynthesis in the sun inferred from the solar-wind ^{7}Li/^{6}Li ratio. *Nature* **402,** 270–273 (1999).
17. Müller, E. A., Peytremann, E. & De La Reza, R. The solar lithium abundance. II. *Solar Phys.* **41,** 53–65 (1975).
18. Schaerer, D., Charbonnel, C., Meynet, G., Maeder, A. & Schaller, G. Grids of stellar models—Part four—from $0.8M_\odot$ to $120M_\odot$ at Z = 0.040. *Astron. Astrophys. Suppl.* **102,** 339–342 (1993).
19. D'Antona, F. & Mazzitelli, I. New pre-main sequence tracks for $M \leq 2.5M_\odot$ as tests of opacities and convection models. *Astrophys. J. Suppl.* **90,** 467–500 (1994).
20. Alexander, J. B. A possible source of lithium in the atmospheres of some red giants. *Observatory* **87,** 238–240 (1967).
21. Ryan, S. G. The host stars of extrasolar planets have normal lithium abundances. *Mon. Not. R. Astron. Soc.* **316,** L35–L39 (2000).
22. Balachandran, S. Lithium depletion and rotation in main-sequence stars. *Astrophys. J.* **354,** 310–332 (1990).
23. Glass, B. P. *Introduction To Planetary Geology* (Cambridge Univ. Press, Cambridge, 1982).
24. Fields, B. D. & Olive, K. A. The evolution of ^{6}Li in standard cosmic ray nucleosynthesis. *New Astron.* **4,** 255–263 (1999).
25. Knauth, D. C., Federman, S. R., Lambert, D. L. & Crane, P. Newly synthesized lithium in the interstellar medium. *Nature* **405,** 656–658 (2000).
26. Thi, W. F. *et al.* Substantial reservoirs of molecular hydrogen in the debris disks around young stars. *Nature* **409,** 60–63 (2001).
27. Levison, H. F., Lissauer, J. J. & Duncan, M. J. Modeling the diversity of outer planetary systems. *Astron. J.* **373,** 1998–2014 (1998).
28. Gonzalez, G., Laws, C., Tyagi, S. & Reddy, B. E. Parent stars of extrasolar planets VI: Abundance analyses of 20 new systems. *Astron. J.* **121,** 432–452 (2001).
29. Boesgaard, A. M. & Tripicco, M. Lithium in early F dwarfs. *Astrophys. J.* **303,** 724–739 (1986).
30. Jones, B. F., Fisher, D. & Soderblom, D. R. The evolution of the lithium abundances of solar-type stars. VIII. M67 (NGC 2682). *Astron. J.* **117,** 330–338 (1999).

Acknowledgements

These observations were made possible through the DDT time granted on the VLT Kueyen by ESO. We thank the Swiss National Science Foundation and the Spanish Ministry of Science and Technology for continuous support for this project. Support from the Fundac ão para a Ciência e Tecnologia, Portugal, and to N.C.S. in the form of a scholarship is acknowledged.

Correspondence and requests for materials should be addressed to G.I. (e-mail: gil@ll.iac.es).

A complementarity experiment with an interferometer at the quantum–classical boundary

P. Bertet, S. Osnaghi, A. Rauschenbeutel, G. Nogues, A. Auffeves, M. Brune, J. M. Raimond & S. Haroche

Laboratoire Kastler Brossel, Département de Physique, Ecole Normale Supérieure, 24 rue Lhomond, F-75231, Paris Cedex 05, France

To illustrate the quantum mechanical principle of complementarity, Bohr[1] described an interferometer with a microscopic slit that records the particle's path. Recoil of the quantum slit causes it to become entangled with the particle, resulting in a kind of Einstein–Podolsky–Rosen pair[2]. As the motion of the slit can be observed, the ambiguity of the particle's trajectory is lifted, suppressing interference effects. In contrast, the state of a sufficiently massive slit does not depend on the particle's path; hence, interference fringes are visible. Although many experiments illustrating various aspects of complementarity have been proposed[3–9] and realized[10–18], none has addressed the quantum–classical limit in the design of the interferometer. Here we report an experimental investigation of complementarity using an interferometer in which the properties of one of the beam-splitting elements can be tuned continuously from being effectively microscopic to macroscopic. Following a recent proposal[19], we use an atomic double-pulse Ramsey interferometer[20], in which microwave pulses act as beam-splitters for the quantum states of the atoms. One of the pulses is a coherent field stored in a cavity, comprising a small, adjustable mean photon number. The visibility of the interference fringes in the final atomic state probability increases with this photon number, illustrating the quantum to classical transition.

Interferences in ordinary space are easier to understand than those of the abstract space of quantum states, so it is illuminating to make the analogy between the Ramsey design[20] and a standard optical interferometer. Instead of Bohr's original design[1] (Fig. 1), we describe here a Mach–Zehnder interferometer[3] which provides a closer analogy with our Ramsey experiment (Fig. 2a). A photon beam is split into two paths *a* and *b* and recombined by two beam splitters B_1 and B_2. The quantum amplitudes associated with these paths present a phase difference ϕ, swept by a retarding element. If B_1 and B_2 are macroscopic, the probability for detecting the particle in detector D exhibits a sinusoidal modulation as a function of ϕ. Suppose now that B_2 is a massive classical object, and B_1 is a light plate rotating around an axis perpendicular to the interferometer

plane. When the particle interacts with B_1, it is, with a 50% probability, either transmitted along path a (the plate does not move) or reflected into path b (the plate receives a momentum kick, resulting in a coherent state of motion). The particle + B_1 system evolves into the combined state:

$$|\Psi> = \left(1/\sqrt{2}\right)(|\Psi_a> |\Psi_{B_1}(a)> + |\Psi_b> |\Psi_{B_1}(b)>) \quad (1)$$

where $|\Psi_a>$ and $|\Psi_b>$ represent the particle's wave packets in paths a and b and $|\Psi_{B_1}(a)>$ and $|\Psi_{B_1}(b)>$ the corresponding final states of B_1. If B_1 is light enough, it stores unambiguous information about the particle's path: $<\Psi_{B_1}(b)|\Psi_{B_1}(a)> = 0$, and $|\Psi>$ is maximally entangled. If B_1 is a heavy macroscopic object insensitive to the particle's momentum kick, $|\Psi_{B_1}(a)> = |\Psi_{B_1}(b)>$ and $|\Psi>$ is an unentangled product state. The probability for detecting the particle in D is:

$$P(\phi) = \tfrac{1}{2}(1 + \mathrm{Re}(<\Psi_{B_1}(b)|\Psi_{B_1}(a)> \exp(i\phi)) \quad (2)$$

The fringe contrast is the modulus of the scalar product of the two beam-splitter final states and directly measures the degree of entanglement between the particle and B_1.

Our Ramsey interferometer, sketched in Fig. 2b, presents an analogy with the Mach–Zehnder device. We describe here only the main features of the set-up; more experimental details can be found elsewhere[21,22]. Rubidium atoms prepared in the circular Rydberg state of principal quantum number 51 (level e) are sent one by one through the interferometer with a velocity of 500 m s^{-1}. Their position is known within 1 mm at all times during their transit across the apparatus. The atoms undergo a transition between e and the lower-energy circular Rydberg level g (principal quantum number 50), at frequency $\nu_{eg} = 51.1$ GHz. This transition is induced by two coherent pulses R_1 and R_2 mixing with equal weights e and g ($\pi/2$ pulses), at two different times separated by a delay $T = 24\ \mu$s. The final atomic energy state is detected in D. The transition probability P_g is reconstructed by averaging a large number of single-atom events.

The pulse R_1 is produced by a small coherent field of complex amplitude α stored in a superconducting Fabry–Perot resonator C (photon damping time $T_{cavity} = 1$ ms). This field is created, before the atom enters the interferometer, by a pulsed coherent microwave source S. The field mode, with a gaussian profile (6 mm waist), is crossed by the atom along a direction perpendicular to the cavity axis. The coherent field state, $|\alpha> = \Sigma_n C_n|n>$, is a superposition of photon numbers with a Poisson distribution. The probability amplitude for having n photons is $C_n = \exp(-|\alpha|^2/2)\alpha^n/\sqrt{n!}$. The mean photon number is $N = |\alpha|^2$, with a variance $\Delta N = \sqrt{N} = |\alpha|$ and a phase fluctuation[3] $\Delta\Phi = 1/|\alpha|$, the minimum value allowed by the Heisenberg uncertainty relation $\Delta N\Delta\Phi \geq 1$.

We determine N by the measurement of the light shift experienced by an auxiliary atom which is crossing the cavity while being non-resonant with its mode[23]. By varying the source amplitude, we tune N from 0 to large values. The $\pi/2$ pulse condition is satisfied by adjusting the duration of the atom–field interaction for each N value. A small electric field is applied between the mirrors of the cavity while the atom is crossing it. In this way, we tune by Stark effect the e–g transition either in or out of resonance with the cavity mode. The atom enters the cavity out of resonance. No evolution occurs until the resonance condition is realised by Stark tuning, at a time such that the $\pi/2$ pulse is achieved when the atom leaves the cavity. The duration of this pulse is a decreasing function of N. The large value of the vacuum Rabi frequency at the cavity centre[24], $\Omega/2\pi = 49$ kHz, ensures that the $\pi/2$ pulse can be achieved even when $N = 0$. The possibility of inducing a $\pi/2$ pulse with the vacuum field, in a time much shorter than T_{cavity}, is an essential feature of cavity experiments with circular Rydberg atoms[25].

After R_1, the combined atom + beam splitter state can be written, in a form similar to equation (1), as:

$$|\Psi> = \left(1/\sqrt{2}\right)(|e> |\alpha_e> + |g> |\alpha_g>) \quad (3)$$

with

$$|\alpha_e> = \sqrt{2}\left(\Sigma_n C_n \cos\left(\Omega\sqrt{n+1}t_\alpha\right)|n>\right)$$
$$|\alpha_g> = \sqrt{2}\left(\Sigma_n C_n \sin\left(\Omega\sqrt{n+1}t_\alpha\right)|n+1>\right) \quad (4)$$

where t_α is an effective atom–cavity interaction time defined by:

$$\Sigma_n |C_n|^2 \cos^2\left(\Omega\sqrt{n+1}t_\alpha\right) = 1/2 \quad (5)$$

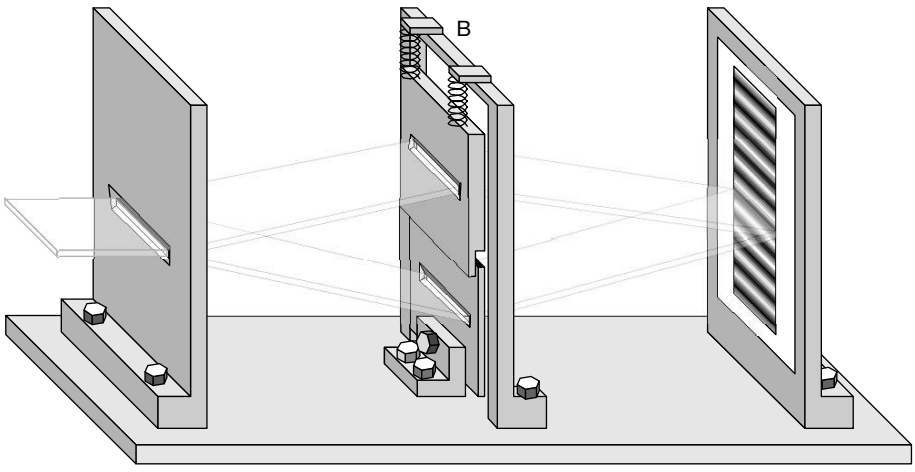

Figure 1 Sketch of an interferometer with a recoiling slit, adapted from Bohr[1]. Particles collimated by the fixed slit at left cross a double slit assembly B and are collected on a detecting plate at right. The bottom slit in B, firmly bolted on the ground plate, cannot move. The upper slit is suspended by springs and assumed to be initially in the ground state of its oscillator motion. When its mass is small enough, the momentum kick imparted by the deflected particle is larger than the initial slit's momentum fluctuations. The state of the slit is entangled with the one of the particle. This provides which-path information and suppresses the interference fringes. When the upper slit is a macroscopic heavy object, its state is not altered by the particle and fringes are observed. By increasing the mass of the slit while keeping the spring stiffness fixed, one could, in principle, continuously span the transition between the two limiting cases discussed by Bohr of a recoiling or fixed slit. The drawing is typical of the semi-serious style adopted by Bohr in his description of thought experiments (in Bohr's original drawings, the various elements were represented separately).

Equation (4) shows that each n-photon component of the coherent state induces a Rabi oscillation between e and g at frequency $\Omega\sqrt{n+1}$[24,25]. The global system's evolution results from the superposition of these Rabi oscillations. In the quantum limit ($N = 0$), $|\alpha_e> = |0>$ and $|\alpha_g> = |1>$ are orthogonal states. In the classical limit, $N \gg 1$, ΔN becomes negligible compared to N. According to equation (5), the $\cos(\Omega\sqrt{n+1}t_\alpha)$ and $\sin(\Omega\sqrt{n+1}t_\alpha)$ functions are approximately $1/\sqrt{2}$, and from equation (4), $|\alpha_e> \approx |\alpha_g> \approx |\alpha>$. The field is thus not significantly altered by the atom. The quantum to classical evolution of the atom–field entanglement described by equation (3) thus exhibits all the qualitative features discussed for the Mach–Zehnder interferometer.

The pulse R_2 is generated by S and fed, via an auxiliary wave guide, into a standing wave independent of C. This standing wave, determined by the structure of the apparatus metallic boundaries, presents an antinode at a distance of 18 mm from the cavity axis. When the atom crosses this antinode, S is switched on for a short time (1 μs), realising the $\pi/2$ pulse condition. The damping time of this standing wave is very short (less than 10 ns). The photons of the R_2 pulse are regenerated many times during the interaction of the atom with this field. Hence, the R_2 field does not get entangled with the atomic state. It can be considered as a classical beam splitter[26] performing the single-particle transformations $|e> \Rightarrow (1/\sqrt{2})(|e> + |g>)$ and $|g> \Rightarrow (1/\sqrt{2})(|g> - |e>)$.

Between R_1 and R_2, the probability amplitudes for finding the atom in e or g accumulate a quantum phase difference ϕ. In order to tune it, we subject the atom to a 2-μs pulse of electric field applied across the cavity mirrors, which shifts the atomic transition frequency and thus ϕ by a variable amount ($0 < \phi < 3\pi$). Taking into account the action of the beam splitters and this phase accumulation, the transition probability between levels e and g may be written as:

$$P_g(\phi) = \tfrac{1}{2}(1 + \mathrm{Re}(<\alpha_e|\alpha_g> \exp(i\phi)) \qquad (6)$$

In Fig. 3a we plot the fringe signals obtained for different amplitudes of the R_1 field, varying from the vacuum ($N = 0$) to $N = 12.8$ ($|\alpha| = 3.5$). In the vacuum case, the fringes are completely washed out: the cavity mode, which undergoes the $0 \Rightarrow 1$ photon transition when the atom flips from e to g, stores 'which path' information. When N increases, the fringes appear, their contrast reaching 72% for $N = 12.8$. This reflects the progressive loss of which-path information, as the beam splitter becomes more and more classical. The maximum fringe contrast is smaller than the ideal 100% given by equation (6), by a factor η due to various experimental imperfections[21,22]. Figure 3b shows the variations of the fringe contrast as a function of N. The points are experimental and the curve represents the theoretical variations of $\eta|<\alpha_e|\alpha_g>|$ where $\eta = 0.75$ is determined by adjusting the theoretical curve on

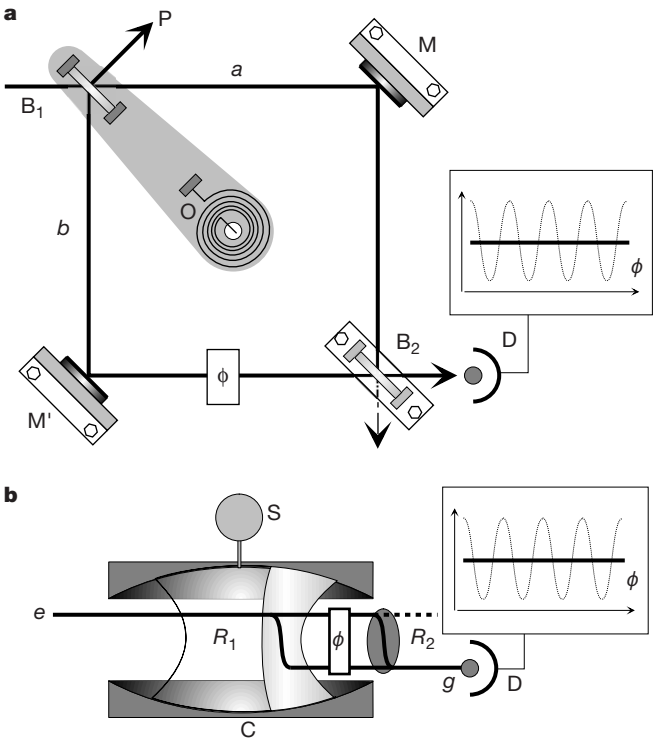

Figure 2 Mach–Zehnder and Ramsey versions of Bohr's experiment. **a**, In the Mach–Zehnder, the particle trajectory is separated by beam splitter B_1 into paths *a* and *b*, folded by mirrors M and M′ and recombined by beam splitter B_2 into detector D. The other output port (dashed arrow) is not used. A dephasing element tunes the relative phase ϕ between the paths. B_1 rotates around an axis perpendicular to the interferometer plane, crossing it at the centre O of the B_1MB_2M' square. A spring provides a restoring force. The moving assembly is initially in its ground state of motion. If B_1 has a large mass, fringes are visible (dotted lines in inset). If B_1 is microscopic, its recoil records the reflection of the particle into path b, washing out the fringes (solid lines). **b**, Ramsey set-up. A Rydberg atom's state is split by microwave pulse R_1 into two energy levels e and g, then recombined by pulse R_2 downstream, before being detected by field-ionization in D. We use a mixed representation combining real space with the space of the atomic energy states. The beam-splitting effect, a spatial separation in the Mach–Zehnder, is now an internal mixture of states. Interferences are obtained in the probability for finding the atom in g. A field pulse between R_1 and R_2 tunes the relative phase ϕ of the interfering amplitudes (Stark effect). If the R_1 field, stored in a long-damping-time cavity C, is macroscopic, Ramsey fringes are visible (dotted line in the inset). If the R_1 field is microscopic, its photon number records information about the atom's path, suppressing the interference (solid line). The gaussian mode of the cavity field is represented schematically; the part where the atom is resonant is shaded. The cavity mode waist and the R_1–R_2 distance are exaggerated.

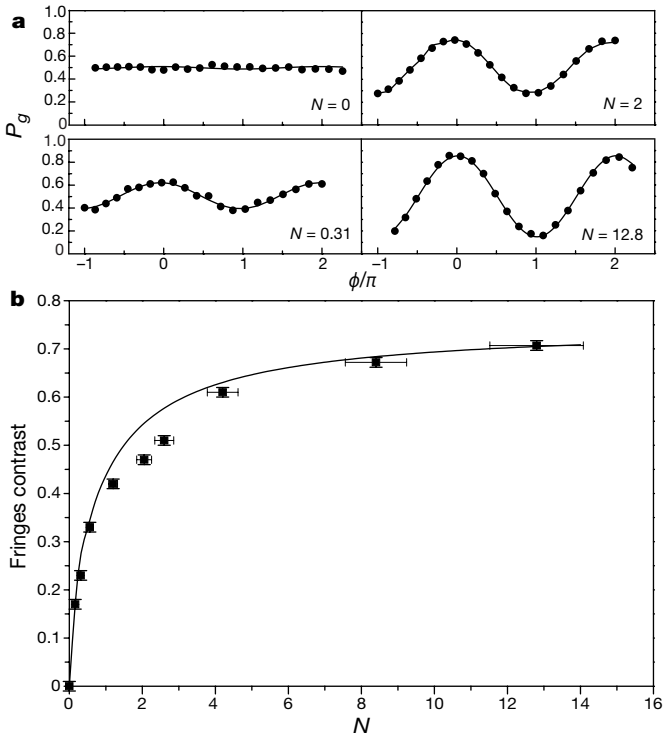

Figure 3 From quantum to classical interferometer. **a**, Ramsey interference signal recorded for various mean photon numbers N in the R_1 pulse. The progressive evolution from the quantum to the classical beam-splitter case is clearly observed. **b**, Fringe contrast as a function of the mean photon number N in R_1. The points are experimental. The line represents the theoretical variation of the modulus of the beam-splitter final-states scalar product, multiplied by a fixed factor η that accounts for interferometer imperfections.

the experimental point at $N = 12.8$. There is excellent agreement between experiment and theory.

Here, as already proposed[4,19], the which-path information is stored in the photon number. It could also be coded in the phase of a coherent field, as suggested[5,27] and demonstrated[28]. In ref. 28, the field interacted in a non-resonant way with Rydberg atoms, between two classical pulses. The atomic index of refraction, which is different for e and g, left the which-path information encoded, not in the photon number, but in the field phase. Contrary to what we observe now (see above), fringes then disappeared for large field amplitudes. The field was then a measuring apparatus, distinct from the interferometer, recording information about the particle's path (that is, its energy) only when it was a classical macroscopic object. Here, the cavity field is part of the interferometer, an apparatus aimed at measuring atomic coherences. The field is a 'well behaved' beam splitter, producing highly contrasted fringes when it contains many photons. Both experiments are in agreement with Bohr's definition of a genuine measuring device, whose parts must be classical.

We can also analyse our experiment in terms of a phase–photon number uncertainty relation. The fringe contrast measures the phase correlation between the two beam splitters, as R_1 imprints its phase on an atomic state superposition, read out later by R_2. The R_2 field has a well defined phase, whereas R_1 presents quantum phase fluctuations $\Delta\Phi$, of the order of $1/\Delta N$. In order to get which-path information, we need $\Delta N < 1$, making a one-photon change in R_1 detectable. This entails $\Delta\Phi > 1$, resulting in the washing-out of phase correlations between R_1 and R_2. The argument is only qualitative here, as the phase is not a real quantum mechanical operator[3] (similar Heisenberg uncertainty arguments, based on the $\Delta x\Delta p > 1$ relation, can be invoked to analyse the Mach–Zehnder thought experiment). In this way, we can easily explain the fringe contrast for $N = 0$ and N large. For intermediate N values, the fundamental atom–R_1 entanglement approach is more precise. Interpreted in a superficial way, the Heisenberg uncertainty explanation seems to describe the R_1–atom interaction as an irreversible noisy perturbation blurring away quantum interferences. This simplistic view is deceptive, however, and the coding of which-path information can be, as we now show, a fully reversible process.

We performed an experiment involving two successive interactions with the same quantum beam splitter, in a configuration such that the which-path information stored during the first interaction was erased during the second, leading to an unconditional restoration of the fringes. The Mach–Zehnder analogue of this experiment is sketched in Fig. 4a and the actual set-up in Fig. 4b. We now assume that the two beam splitters are microscopic quantum plates rigidly coupled together by a rotating assembly moving around O. The B_1 and B_2 plates are kicked when the particle follows the paths b and a, respectively, resulting in both cases in the same final rotation of the assembly (arrows in Fig. 4a). The which-path information acquired by B_1 is 'erased' when the particle reaches B_2, a situation reminiscent of the 'quantum eraser'[3,17,19,29,30]. The fringes should then be visible. In usual quantum-eraser procedures, however, the which-path recording system is actively manipulated, then measured. Conditional interferences appear, whose phase depends upon the outcome of the which-path detector measurement. If this measurement is not performed, fringes do not show up. Here, on the contrary, the information is unconditionally erased by the second interaction with the beam splitter.

The Ramsey version of this experiment (Fig. 4b) involves two successive pulses induced by the quantum field in C. The cavity is initially in vacuum state. The first pulse occurs when the atom enters the mode waist and the second just before it leaves the waist, a time $T = 16\,\mu$s later. The interaction with the quantum field is interrupted in between by Stark switching. An additional 2-μs pulse of electric field is used, as in the previous experiment, to sweep the phase difference ϕ between the two paths. The first Ramsey pulse transforms the atom + field state into the entangled superposition described by equation (3) with $|\alpha_e> = |0>$ and $|\alpha_g> = |1>$. The interferometer then stores which-path information. Just before the second pulse, the atom + field system is in the combined state:

$$|\Psi'> = \left(1/\sqrt{2}\right)(\exp(i\phi)|e>|0> + |g>|1>) \qquad (7)$$

The second quantum pulse mixes again coherently $|e, 0>$ and $|g, 1>$ transforming this superposition into:

$$|\Psi''> = \tfrac{1}{2}[|g>|1>(1 + \exp(i\phi)) - |e>|0>(1 - \exp(i\phi))] \quad (8)$$

The system's state contains two terms corresponding to the atom ending up in g, with a phase difference ϕ between them. In both terms, the field is in the same one-photon state. The likeness to the Mach–Zehnder case is noticeable: the photon in the cavity replaces the momentum kick stored in the beam-splitter assembly. The final

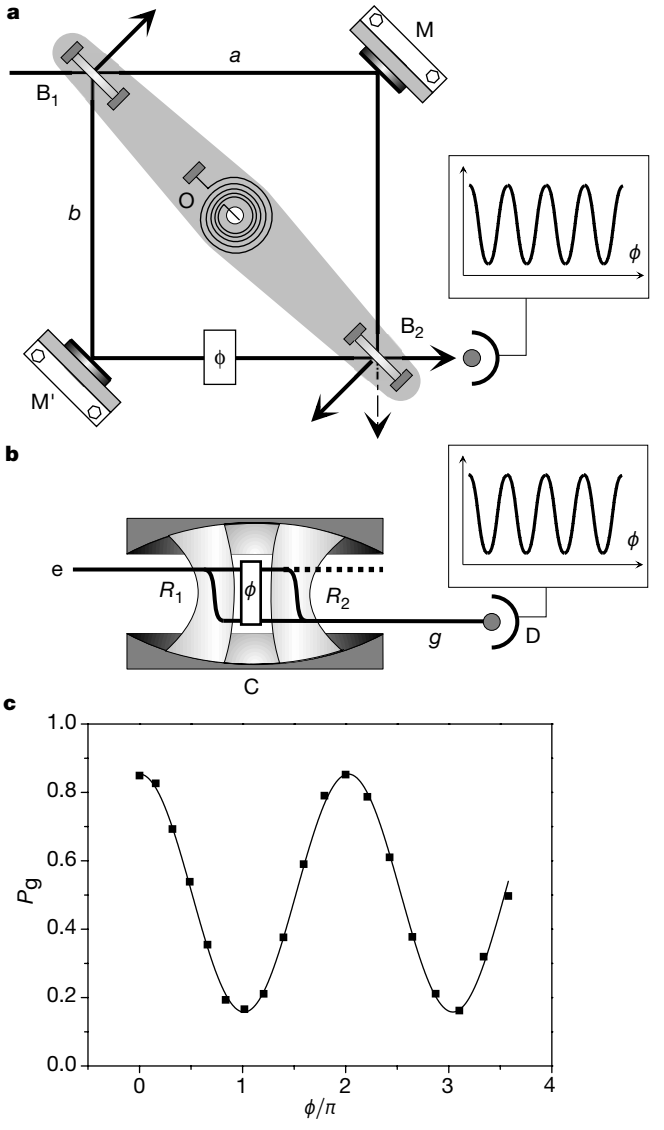

Figure 4 The unconditional quantum-eraser experiment. **a**, Mach–Zehnder's version: B_1 and B_2 are rigidly coupled to the same assembly rotating around O. Both paths result in the same angular momentum kick of the B_1–B_2 system. Fringes should appear. **b**, Actual Ramsey experiment. R_1 and R_2 are produced by the same quantum mode in C, initially empty. The coupling of the atom is interrupted between R_1 and R_2 by Stark switching. In both paths ending in level g, the atom finally releases one photon in C: the which-path information, produced by the first pulse, is 'erased' by the second. **c**, Interference signal obtained under these conditions exhibiting a large fringe contrast.

information contained in the field does not distinguish the two paths leading to g. The two corresponding amplitudes interfere. This results in large contrast fringes on P_g, as shown in Fig. 4c. We note that these fringes are visible despite the overall random phase of the pulses. The fringe contrast is sensitive to the phase correlation of the Ramsey fields between the times 0 and T, which is non-vanishing as long as $T < T_{\text{cavity}}$.

We have shown that a coherent field stored in a low-loss cavity realises a versatile beam splitter for atomic interferometry experiments. It can evolve continuously from a microscopic device, able to store which-path information, into a macroscopic system with a large number of quanta, insensitive to the interaction with the interfering particle. When the beam splitter is quantum, its coupling with the particle results in maximum entanglement between the two systems. When the same quantum beam-splitter is used twice in the interferometer, the quantum information is erased and the fringes restored. By allowing us to explore the transition from microscopic to macroscopic measuring devices, these experiments shed light on the quantum-classical boundary. □

Received 22 December 2000; accepted 7 March 2001.

1. Bohr, N. in *Albert Einstein: Philosopher Scientist* (ed. Schilpp, P. A.) 200–241 (Library of Living Philosophers, Evanston, 1949); reprinted in *Quantum Theory and Measurement* (eds Wheeler, J. A. & Zurek, W. H.) 9–49 (Princeton Univ. Press, Princeton, 1983).
2. Einstein, A., Podolsky, B. & Rosen, N. Can quantum mechanical description of physical reality be considered complete? *Phys. Rev.* **47,** 777–780 (1935).
3. Scully, M. O. & Zubairy, M. S. *Quantum Optics* (Cambridge Univ. Press, Cambridge, UK, 1997).
4. Scully, M. O., Englert, B. G. & Walther, H. Quantum optical tests of complementarity. *Nature* **351,** 111–116 (1991).
5. Haroche, S., Brune, M. & Raimond, J. M. Manipulations of optical fields by atomic interferometry: quantum variations on a theme by Young. *Appl. Phys. B* **54,** 355–365 (1992).
6. Englert, B. G. Fringe visibility and which-way information: an inequality. *Phys. Rev. Lett.* **77,** 2154–2157 (1996).
7. Englert, B. G., Scully, M. O. & Walther, H. Complementarity and uncertainty. *Nature* **375,** 367 (1995).
8. Storey, P., Tan, S., Collet, M. & Walls, D. Complementarity and uncertainty. *Nature* **375,** 368 (1995).
9. Wiseman, H. *et al.* Non local momentum transfer in welcher Weg measurements. *Phys. Rev. A* **56,** 55–75 (1997).
10. Badurek, G., Rausch, H. & Tuppinger, D. Neutron interferometric double resonance experiments. *Phys. Rev. A* **34,** 2600–2608 (1985).
11. Grangier, P., Roger, G. & Aspect, A. Experimental evidence for photon anticorrelation effect on a beam splitter: a new light on single-photon interference. *Europhys. Lett.* **1,** 173–179 (1986).
12. Pfau, T. *et al.* Loss of spatial coherence by a single spontaneous emission. *Phys. Rev. Lett.* **73,** 1223–1227 (1994).
13. Chapman, M. S. *et al.* Photon scattering from atoms in an atom interferometer: coherence lost and regained. *Phys. Rev. Lett.* **75,** 3783–3787 (1995).
14. Eichman, U. *et al.* Young's interference experiment with light scattered from two atoms. *Phys. Rev. Lett.* **70,** 2359–2362 (1993).
15. Dürr, S., Nonn, T. & Rempe, G. Origin of quantum-mechanical complementarity probed by a "which way" experiment in an atom interferometer. *Nature* **395,** 33–37 (1998).
16. Dürr, S., Nonn, T. & Rempe, G. Fringe visibility and which-way information in an atom interferometer. *Phys. Rev. Lett.* **81,** 5705–5709 (1998).
17. Herzog, T. J., Kwiat, P. G., Weinfurter, H. & Zeilinger, A. Complementarity and the quantum eraser. *Phys. Rev. Lett.* **75,** 3034–3037 (1995).
18. Bucks, E., Schuster, R., Heiblum, M., Mahalu, D. & Umansky, V. Dephasing in electron interference by a "which-path" detector. *Nature* **391,** 871–874 (1998).
19. Zheng, S. B. A simplified scheme for testing complementarity and realising quantum eraser. *Opt. Comm.* **173,** 265–267 (2000).
20. Ramsey, N. *Molecular Beams* (Oxford Univ. Press, Oxford, UK, 1985).
21. Nogues, G. *et al.* Seeing a single photon without destroying it. *Nature* **400,** 239–242 (1999).
22. Rauschenbeutel, A. *et al.* Coherent operation of a tunable quantum phase gate. *Phys. Rev. Lett.* **83,** 5166–5169 (1999).
23. Brune, M. *et al.* From Lamb shift to light shifts: vacuum and sub-photon cavity fields measured by atomic interferometry. *Phys. Rev. Lett.* **72,** 3339–3342 (1994).
24. Brune, M. *et al.* Quantum Rabi oscillation: a direct test of field quantization in a cavity. *Phys. Rev. Lett.* **76,** 1800–1803 (1996).
25. Haroche, S. & Raimond, J. M. in *Cavity Quantum Electrodynamics* (ed. Berman, P.) 123–170 (Academic, New York, 1992).
26. Kim, J. I. *et al.* Classical behaviours with small quantum numbers: the physics of Ramsey interferometry of Rydberg atoms. *Phys. Rev. Lett.* **82,** 4737–4740 (1999).
27. Gerry, C. C. Complementarity and quantum erasure with dispersive atom-field interaction. *Phys. Rev. A* **53,** 1179–1182 (1996).
28. Brune, M. *et al.* Observing the progressive decoherence of the meter in a quantum measurement. *Phys. Rev. Lett.* **77,** 4887–4890 (1996).
29. Scully, M. O. & Srühl, K. Quantum eraser: a proposed photon correlation experiment concerning observation and "delayed choice" in quantum mechanics. *Phys. Rev. A* **25,** 2208–2213 (1982).
30. Kwiat, P. G., Steinberg, A. M. & Chiao, R. Y. Observation of a "quantum eraser": a revival of coherence in a 2-photon interference experiment. *Phys. Rev. A* **45,** 7729–7739 (1992).

Acknowledgements

Laboratoire Kastler Brossel is Unité Mixte de Recherches of Ecole Normale Supérieure, Université P. et M. Curie and Centre National de la Recherche Scientifique. This work was supported by the Commission of the European Community and by the Japan Science and Technology Corporation (International Cooperative Research Project, Quantum Entanglement Project).

Correspondence and requests for materials should be addressed to S.H. (e-mail: haroche@lkb.ens.fr).

Semiconducting non-molecular nitrogen up to 240 GPa and its low-pressure stability

Mikhail I. Eremets, Russell J. Hemley, Ho-kwang Mao & Eugene Gregoryanz

Geophysical Laboratory and Center for High Pressure Research, Carnegie Institution of Washington, 5251 Broad Branch Road NW, Washington DC 20015, USA

The triple bond of diatomic nitrogen has among the greatest binding energies of any molecule. At low temperatures and pressures, nitrogen forms a molecular crystal in which these strong bonds co-exist with weak van der Waals interactions between molecules, producing an insulator with a large band gap[1]. As the pressure is raised on molecular crystals, intermolecular interactions increase and the molecules eventually dissociate to form monoatomic metallic solids, as was first predicted for hydrogen[2]. Theory predicts that, in a pressure range between 50 and 94 GPa, diatomic nitrogen can be transformed into a non-molecular framework or polymeric structure with potential use as a high-energy-density material[3–5]. Here we show that the non-molecular phase of nitrogen is semiconducting up to at least 240 GPa, at which pressure the energy gap has decreased to 0.4 eV. At 300 K, this transition from insulating to semiconducting behaviour starts at a pressure of approximately 140 GPa, but shifts to much higher pressure with decreasing temperature. The transition also exhibits remarkably large hysteresis with an equilibrium transition estimated to be near 100 GPa. Moreover, we have succeeded in recovering the non-molecular phase of nitrogen at ambient pressure (at temperatures below 100 K), which could be of importance for practical use.

McMahan and LeSar[3] first predicted that nitrogen would transform from the molecular state, in which each atom is triple-bonded with one near neighbour, to a monoatomic structure in which each atom is bonded to three nearest neighbours by single covalent bonds. This unusual transition is also interesting from the point of view of the chemistry of nitrogen and its applications. Only small molecules with two or three nitrogen atoms in a row are known (the only exception being perhaps $N_5^+AsF_6^-$; ref. 6). These may form high-energy-density materials because the transformation from polymerized nitrogen to diatomic molecular nitrogen is accompanied by a very large energy release[6] (the average bond strength of the N–N single bond is 160 kJ mol^{-1} and that of the triple bond is 954 kJ mol^{-1}). The calculations[3–5] predicted this transformation to occur at pressures of 50–94 GPa with a large volume change of approximately 35%; this prediction has been examined in additional detail in numerous subsequent theoretical studies[7–10]. The electronic properties of non-molecular nitrogen strongly depend on the particular crystalline structure. Many structures have been considered[3–5]; the lowest-energy modifications reported seems to